NTNU
Norwegian University of
Science and Technology

Digital Twin of Crane

Erlend Erdal Christiansen

Abstract

This master thesis aims to make a digital twin of a crane for structural monitoring. A digital twin is any physical structure or mechanical system (asset) that is monitored and inspected by a digital model. Fedem, which is a simulation program for dynamic mechanisms, is used for the digital twin. One of the main tasks is to synthesize an inverse method to capture the load applied to the crane. This is done by detecting the strain in the outer boom, consisting of bending strain and normal strain induced by the applied load. With use of equilibrium equations a mathematical model estimates the load based on these strains. Strain gauges are mounted to the crane and the data are used for the estimations. In a static test the load is estimated with a deviation less than 2% from the applied load. Dynamic testing also shows promising results. The other main task is to benchmark the responses of the digital model. Strain gauges on the crane and virtual strain gauges on the model are used to compare the responses. A standard 3D test runs is used as a basis for the bechmarking. The Fedem model is tuned to make the response more similar to the physical crane. The results of the benchmarking shows that there are still work to be done on the model before the responses are within a acceptable margin.
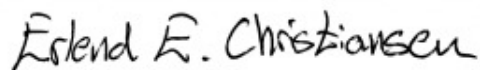
Sammendrag

Denne masteroppgåva har som mål å lage ein digital tvilling av ei kran for strukturell monitorering. Ein digital tvilling er kva som helst slags fysisk konstruksjon eller mekanisk system som monitorerast og inspiserast av ein digital modell. Fedem, som er eit simuleringsprogramm for dynamiske mekanismer, er brukt til den digitale tvillingen. Ei av hovudoppgåvene er å utvikle ein inversmetode for å finne lasta som er sett på krana. Dette er gjort ved å detektere tøyningane i den ytre bommen, som består av tøyningar frå bøying og normaltøyningar, indusert av den påsette lasta. Ved bruk av likevektslikningar er ein matematisk modell sett opp som estimerer lasta basert på desse tøyningane. Strekklappar er montert på krana og data frå desse er brukt til estimasjonen. I ein statisk test er lasta estimert til å ha eit avvik som er mindre enn 2% ut i frå den påsette lasta. Dynamisk testing viser også gode resultat. Den andre hovudoppgåva er å vurdere kvaliteten på responsen som den digitale modellen gjev. Strekklappar på krana og virtuelle strekklappar i modellen er brukt for å samanlikne responsen. Ei standard 3D testkjøring er brukt som ein basis for vurderinga. Modellen i Fedem er justert for å ein respons som er nærmare responsen til den fysiske krana. Resultatet frå desse vurderingane er at meir arbeid må leggast ned i modellen for at responsen skal komme innanfor ein akseptabel margin.

Preface

This master thesis marks the end of the master program of mechanical engineering at Norwegian University of Science and Technology, NTNU, in Trondheim. It has been exciting to gain insight to a field in development and inspiring to see where the technology is heading. Working with this thesis has been a challenging exercise and required me to use the knowledge gathered throughout my time at the university. Also new knowledge was gained and new experiences made.

I would like to thank my supervisor, Terje Rølvåg, for supporting me throughout this whole process. He was very helpful with the modeling of the crane and quickly answered my calls and texts. A thank you also goes to Halvard Støwer who helped me with the instrumentation of the crane, as well as getting the equipment needed to do the job. He also learned me a lot about the field, which I had limited previous experiences with. At last I want to thank PHD student Andrej Cibicik for letting me use the crane he has made for research purposes. He helped out with operating it and contributed with a lot of useful input for my thesis.

Ulsteinvik, September 7th, 2018

Erlend E. Christiansen

Contents

List of Figures

List of Tables

1   Introduction

In this thesis the goal is to make a digital twins solution for the crane seen in figure 1. It consists of several tasks with the ultimate goal of making a digital twin that can be used to monitor the structural integrity of the crane. It is built at one of the NTNU departments and is used for research purposes. This makes it an ideal use case to benchmark a digital twins solution.
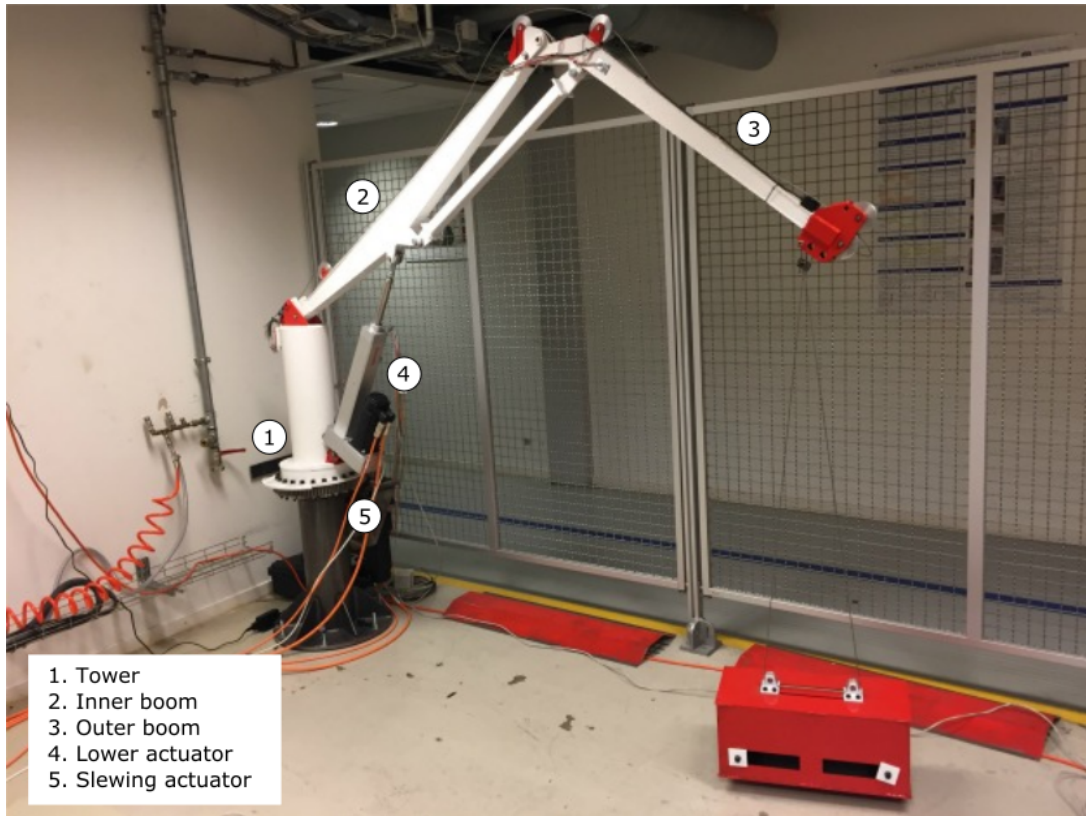
Figure 1: The crane

1.1   Background

Recently a lot of hype has been given to buzzwords like IOT and digital twins, and the expectations of what this can lead to is high [1]. However, the technologies are yet to be matured and a lot of big players are expected to compete to be the first to deliver results that will bring value to the end users. A digital twin is any physical structure or mechanical system (asset) that is monitored and inspected by a digital model.

1.2 Approach

The ultimate goal is to make a digital twins solution for the crane. Fedem, which is a simulation program for dynamic mechanisms, is used for the digital twin. A copy of the task description can be found in appendix A.1. The process is divided into several steps and the objectives of the thesis are listed below.

1. Update the FEDEM crane model (structures, wires, control systems, sensors and actuators)

2. Identify an optimal distribution of sensors to capture the applied payload and responses

3. Develop inverse method to synthesize applied loads based on physical sensor outputs

4. Instrument the crane based on results from task 2

5. Setup and benchmark the virtual and physical crane

6. Evaluate how well the sensors and inverse method are capturing the payload on the physical crane

The thesis really consists of two main tasks that the other objectives helps to achieve. One is to capture the load based on an inverse method. The approach used is to measure the strains in the outer boom of the crane. Based on the bending strain and normal strain, the load can be calculated when the position of the boom is known. The model of the crane and instrumentation of the physical crane have been setup for this purpose. The other main task is to match the response of the model to the response of the physical crane. To evaluate this, the approach of using a standard 3D test run was chosen. By doing this, the digital twins solution can be benchmarked before communication is set up at a later time.

1.3 Structure of the report

The structure of the report is here described briefly chapter by chapter to give an overview of the contents of the report. Chapter 2 concerns the digital part of twin. The crane is modeled in Fedem with mechanisms and functions defined by a standard 3D test run. It is described how the model has been tuned to mimic the response of the physical crane. Chapter 3 describes the instrumentation of the crane. It argues on the position of the sensors for the inverse method and the benchmarking. It also documents the setup of the sensing system. Chapter 4 compares the natural frequencies of the crane with results from a modal analysis in Fedem. In chapter 5, the inverse method is developed. It presents the mathematical model used to synthesize the loads and check the accuracy of the model by a static test. In chapter

6 the results from the standard 3D test run is presented. It compares the virtual and physical strain gauges and the calculated and simulated load. The discussion of the results are also presented in the same chapter. Finally chapter 7 suggest the further work on the digital twin.

2 Fedem crane model

In this section the digital model of the crane is documented. It describes the preparations done in Siemens NX, and the mechanisms added in Fedem. The functions applied to the model are presented, making the crane move according to a defined test run and at the end it describes the setup of the simulation. Figure 2 displays the model of the crane in Fedem.
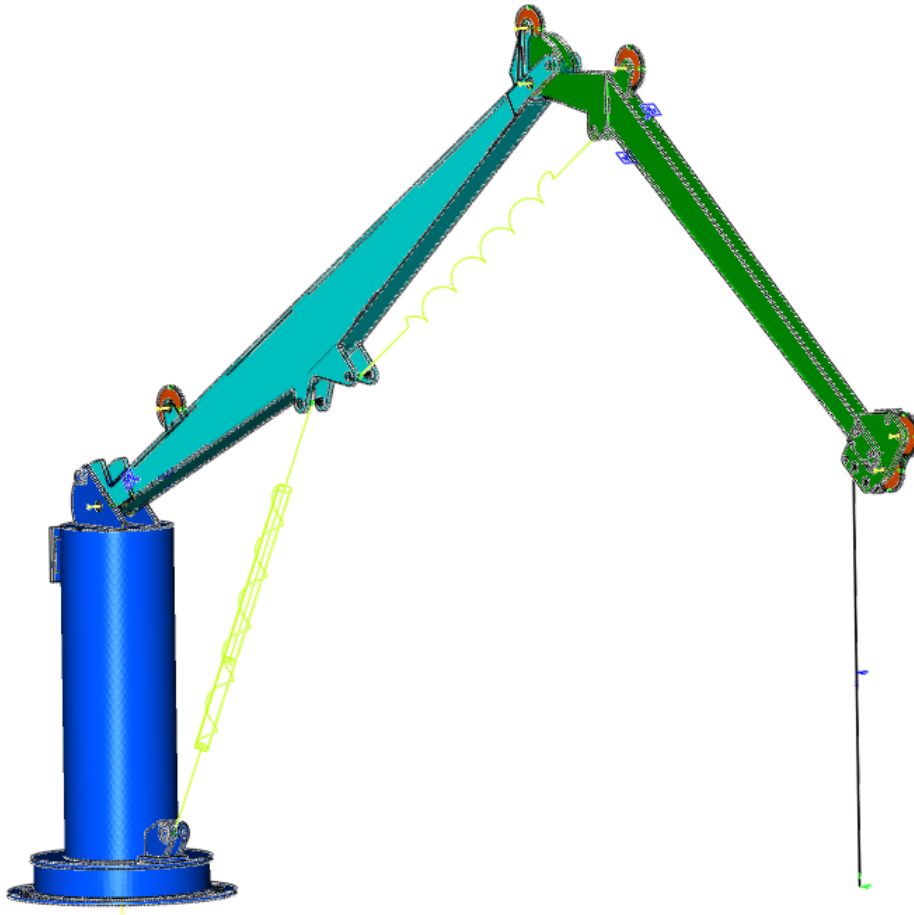

Figure 2: Model of the crane in Fedem

2.1 Preparations in Siemens NX

A detailed 3D- model of the crane was provided to be used as the virtual model of the crane, but welds were not included in the model. Because all of the parts of the crane are fully welded it was important to include this in the model, as it makes a difference to the stiffness of the construction. It is important to make the physical and virtual crane as equal as possible to be able to capture the wanted response from the virtual model.

The crane was meshed with CTETRA10 elements. This element is in the shape of a tetrahedron and has 10 nodes. The two booms are meshed with one element across the thickness of the plates. The length of the elements are set to be about 5 mm at the areas where the virtual strain gauges are positioned. This is done to match the physical strain gauges which have a gauge length of 5 mm. In the holes of all parts that have joints or other connections in Fedem, RBE2 elements was added. This is a rigid body element for rigid connections, with master and slave elements.

The material is also assigned is Siemens NX. This material is inherited by Fedem when the files are imported. The material used is steel with an elastic modulus of 206 GPa. The Poisson's ratio is set to 0.3 and the density of the material is 7850 kg/m^3.

2.2 Mechanisms in Fedem

Figure 3 displays the Fedem model of the crane with positions of the different mechanisms used.

(A) Position A marks the hinges connecting the parts of the crane. They are modeled with revolute joints. The joints have one rotational degree of freedom and the constraint type is set to free. This makes the hinges move freely as the lower actuator changes length.

(B) Position B marks the connection between the booms and the pulleys. These are also modeled with revolute joints, but the pulleys can not rotate freely about its degree of freedom. It is modeled with a spring- damper constraint type. This is done so that the pulleys will not rotate during the simulation. The stress free angle control is set to zero deflection and the stiffness in the spring properties is set to 10^9. No damping is added.

(C) Position C marks the revolute joint connecting the tower to the ground. This joint represents the slewing actuator of the system. It also has a spring-damper type of constraint with the same stiffness as the pulleys. The slewing actuator function is set for the stress free angle change, making the crane rotate according to the function.

(D) Position D marks the two springs used in the model. The one to the right in the figure has a constant length and represents the rigid bar on the crane. The spring to the left represents the lower actuator on the crane. The stress free length change of this spring is dictated by the lower actuator function. The stiffness of the springs are set to 10^8. Next to the spring representing the lower actuator, a damper can be seen. This damper ended up not being used.

(E) Position E marks the position of the virtual strain gauges. The rosette type used is triple gauge 45 degrees. They are positioned at the same points as the physical gauges. The virtual strain gauge to the left in the figure is one of two on this boom. The other one is on the back side at the same spot. This is also were the physical gauge is mounted. The gauges in this position are used for benchmarking the accuracy of the model. The two virtual gauges to the right are used for the inverse method, and were also used to tune the model to match the physical results in the same position.

(F) Position F marks the wire connecting the load to the crane. In the bottom end it is connected to the triad that is plotted by the payload function. The length of the wire is the same as the length used in the physical testing, 0.731 m. The cross section of the wire is circular with a diameter of 1 mm. The material is steel with an elastic modulus of 210 GPa, poisson's ratio of 0.29, density of 7850 kg/m^3 and a shear modulus of 81.4 GPa. The wire stiffness was estimated physically and is presented later.
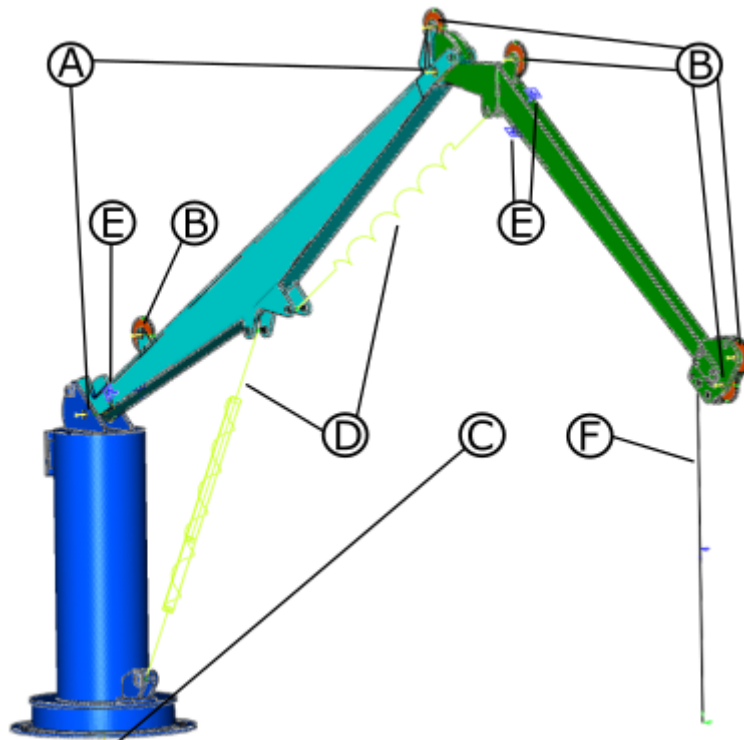
Figure 3: Position of mechanisms in the Fedem model

2.3   Measuring wire stiffness

In order to get reasonable oscillations in the 3d- model of the crane, the beam that connects the load to the boom needs a representative stiffness. This stiffness could be found by doing a tension test of the wire and then calculate the resulting stiffness in the configuration used on the crane, as seen in figure 4. A simpler method was used because it was more efficient and because it gives the resulting stiffness directly instead of doing extra calculations.

Figure 4: Setup for measurement of wire stiffness

By using hookes law the stiffness of the wire setup can be found. The stiffness K is a function of the change in force with respect to change in length.

$$F = kx \qquad (1)$$

$$k = \frac{F}{x} \qquad (2)$$

The mass of the load was measured by a scale with resolution 50 grams. This scale was connected to a crane and the load with the wire was connected to the scale. Taped to the scale was a device measuring distance with a laser. The resolution was 0.1 mm. The goal was to first measure the distance down the the top of the box that represents the mass. This was done by rising the crane until there was no slack in the wire. The pretension was for all tests done at approximately 15.5kg. When the system was at rest the distance was measured. The the entire mass of 30.6 kg was lifted of the ground. When the system came to rest the new distance was measured. Several test was conducted to see if the results was reliable. On the basis of these measurements the stiffness was approximate do be as follows.

$$k = \frac{15kg \times 9.81m/s^2}{0.0013m} = \underline{\underline{113kN/m}} \qquad (3)$$

This calculation must be seen as a approximation due to the many uncertainties of the measuring setup. When the entire mass was lifted from the ground it may have been tilted from being unbalanced. The laser may have been shifted due to not being completely fixed the the scale. The point that was measured was fairly the same but a small deviation could possibly have affected the result.

2.4   Standard 3D test run

To be able to compare test results from physical testing with simulations, a standard 3D test run was established to use as a basis. This is also used for fatigue calculations.

1. The crane starts of at rest, as seen to the right in figure 5. At this position the lower actuator has a length of 0.873150 meters measured from the center of each of the two connection points.

2. The crane then tilts upward by changing the length of the lower actuator with a constant speed. The movement lasts for nine seconds, resulting in an actuator length of 0.9481 meters.

3. Tilting stops and a one second break follows.

4. The slewing actuator rotates the crane clockwise for ten seconds. At constant velocity it slews to a final position of 0.853 radians relative to the starting position.

5. Slewing stops and another break of one second follows.

6. The lower actuator then contracts, tilting the crane down. The landing lasts for 9.5 seconds resulting in a lower actuator length of 0.869 meters.

7. Tilting stops and the motion breaks for five seconds.

8. The crane then tilts back up, rotates counter clockwise and tilts back down. The motion is the same as in point 1 to 7, but in a reverse order.
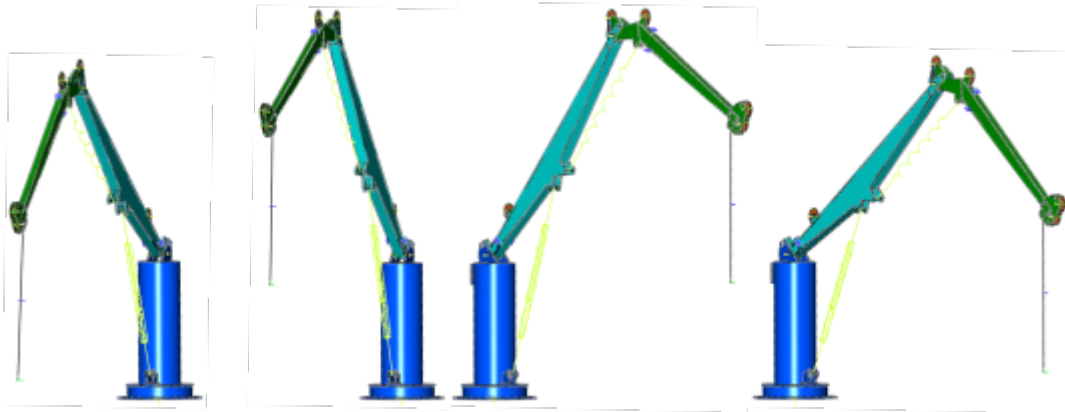

Figure 5: Visualization of standard test run

2.5 Functions

Functions are made in Fedem to follow the standard 3D test run. These functions are in turn added to the spring, revolute joint and triad that represents the actuators and payload. The functions are set up as polylines with time as the argument. The time and value are added for each point the function value changes, and the change between two points is linear. The parameters are added based on the standard 3D test run.

The functions for the actuator motions are processed by a control system. The control systems used, are displayed in figure 6. The aim of it is to smooth out the acceleration that happens when the function goes from one speed to another. The functions are the input to the left in the figure. They go through the smoothing in the centre, before they reach the output. The value of K is set to one while different values for T_s was tried to see what matched the response from the physical testing best. Only the control system for the slewing actuator ended up to be used, with a value T_s equal to 0.2.
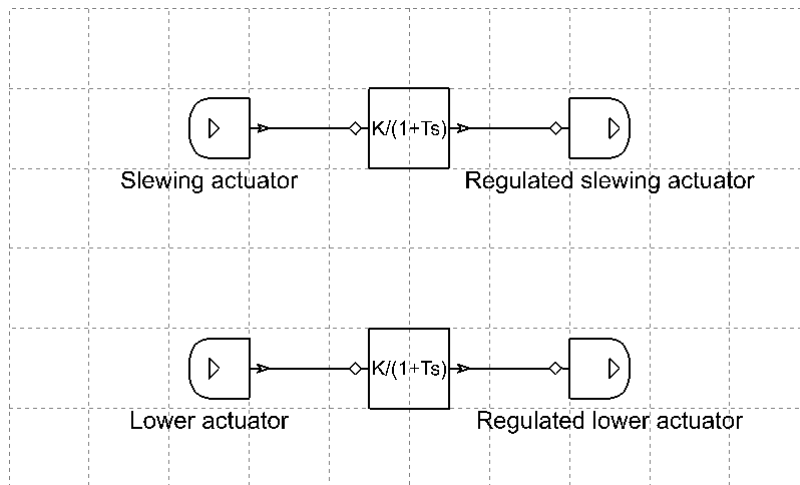
Figure 6: Control editor in Fedem

2.6 Simulation setup

The dynamic solver was setup to preform equilibrium iterations at initial position. This is important when comparing the simulation solutions to the results from physical testing. The strain gauges in the physical testing was set to zero when the crane was carrying its own weight. This is also what the solver does when initial equilibrium is found. The simulation runs from 0- 70 seconds with a time step of 0.002 seconds. Newmark integration with numerical damping is used with a HHT-alpha factor of 0.1.

3   Instrumentation

In this chapter the instrumentation of the crane is described. First the positioning of the strain gauges are identified with the concern to the inverse method and the hotspot for benchmarking. Then it gives insight to the equipment used and the different steps needed to implement the instrumentation and getting it ready. Finally it explains the choice of using strain rosettes on the crane. Figure 7 shows the instrumented crane. At position A four strain rosettes are placed on each side of the beam. At position B the strain rosette for the benchmarking is positioned on the backside of the beam.

Figure 7: The crane with instrumentation

3.1 Identifying distribution of strain gauges for inverse method

The task is to capture the load applied to the crane by an inverse method. Using strain gauges, the bending strain in the outer boo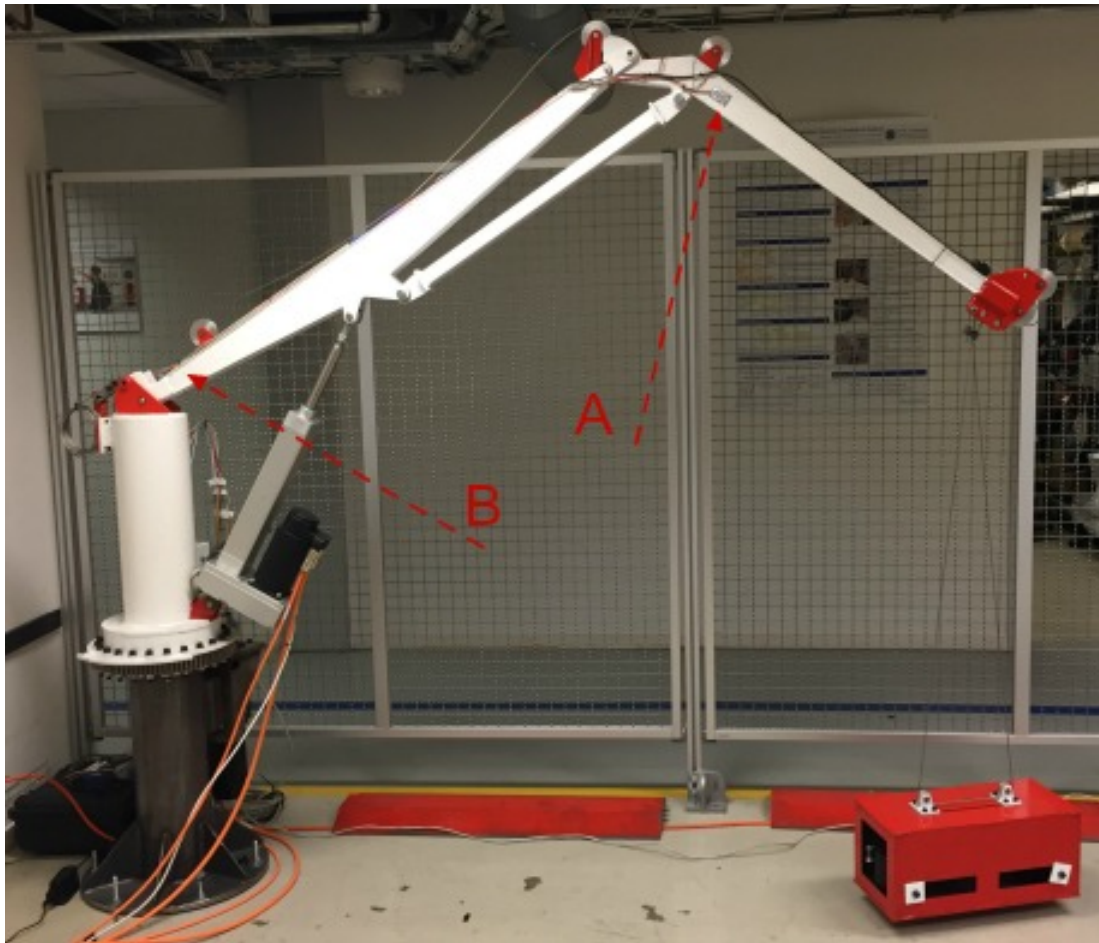m can be detected and the load calculated. To do this the strain gauges has to be positioned on the crane in a way that gives good measurements. The largest strains occur where the bending stresses are highest and is therefore a good spot. A simplified model of the crane can be seen in figure 8. The crane is represented as a wire model and a force, F, is applied to the tip of the outer boom. This beam has an angle, α, relative to the horizontal plane. To find the best place to position the strain gauges only the outer boom needs to be evaluated, and a model of this part is illustrated in the figure. The model can be viewed as a type of cantilever beam that is statically indeterminate. It has one extra bearing force in the horizontal direction, resulting in being one equilibrium equation short. However for this analysis only the vertical forces will be taken into account. Also the area of interest is to the right of the bearings. This is because the bending moment will be the main source for strain in the construction and since the goal is to find the load, the area around the bearings should be avoided. The force, F, can be decomposed into two components. One acting parallel two the cantilever beam and one acting perpendicular. As illustrated in the figure the angle, α, and the force, F, at the hypotenuse makes up a right triangle along with two legs. These two legs are the decomposed forces resulting in the equations 4.

$$
\begin{aligned}
F_H &= F sin\alpha \\
F_V &= F cos\alpha
\end{aligned}
\tag{4}
$$
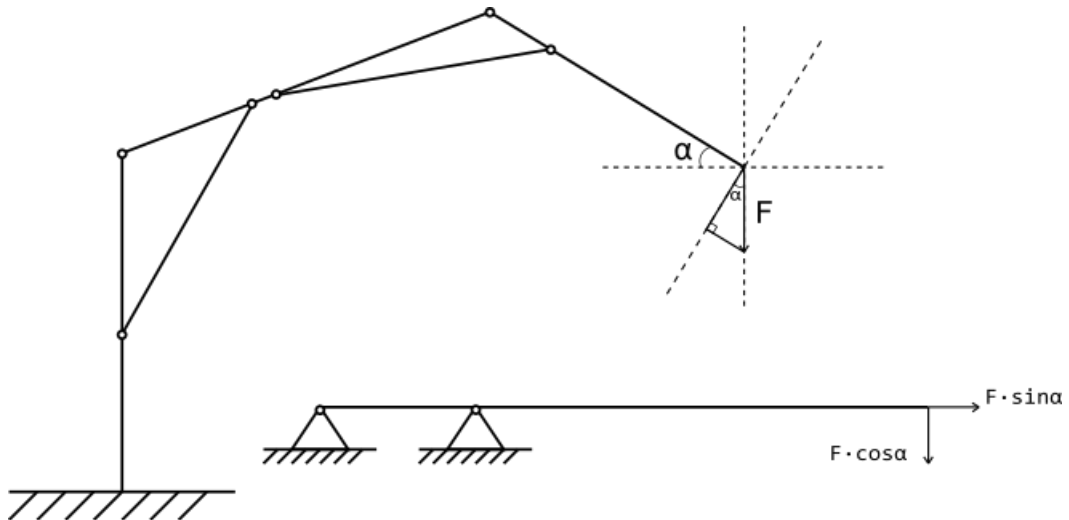
Figure 8: Simplified wire model of the crane

14

Intuitively the largest bending stresses should be over the right bearing, but the cross sectional area is not constant. It varies linearly along the length of the beam. To make sure the desired area of the beam is used, the bending stress is plotted as a function of the length of the beam with respect to the bending moment and the varying cross section. The bending stress relation is shown in equation 5 and the final function in equation 7. The values used in the calculation are displayed in figure 9.

$$\sigma = \frac{M(x)}{I}y$$
$$\sigma = \frac{Fx}{\frac{1}{12}b_y h_y^3 - \frac{1}{12}b_i h_i^3}\frac{h_y}{2} \tag{5}$$

where

$$h_y = h_y(x) = h_{0y} + \frac{x}{L}h_1$$
$$h_i = h_i(x) = h_{0i} + \frac{x}{L}h_1 \tag{6}$$

resulting in

$$\sigma = \frac{6Fx}{b_y(h_{0y} + \frac{x}{L}h_1)^3 - b_i(h_{0i} + \frac{x}{L}h_1)^3}(h_{0y} + \frac{x}{L}h_1) \tag{7}$$
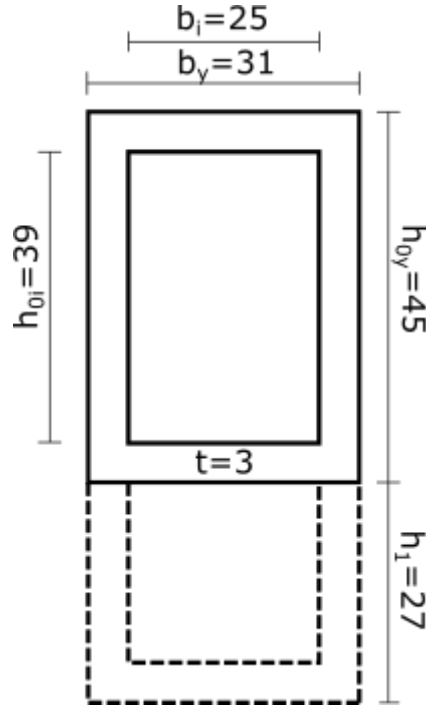
Figure 9: Simplified cross sectional area of the outer boom

15

Plotted in figure 10 is the relation between the bending stress along the length of the beam. The force, F, used in this analysis is 500N and a length, L, of 830mm. Starting at zero, which represents the tip of the beam, the bending stress increases. Even though the effects of the varying cross section is present, the bending stress is still the highest furthest away from the tip where the load is applied. Based on these results a good spot to place the strain gauges is near the bearings, but not too close to avoid any effects that may interfere, such as notches. In this part of the beam the cross sectional area is larger than on the tip, meaning the effects of normal stresses are the smallest. This is also an advantage, making the inverse method mostly about pure bending.
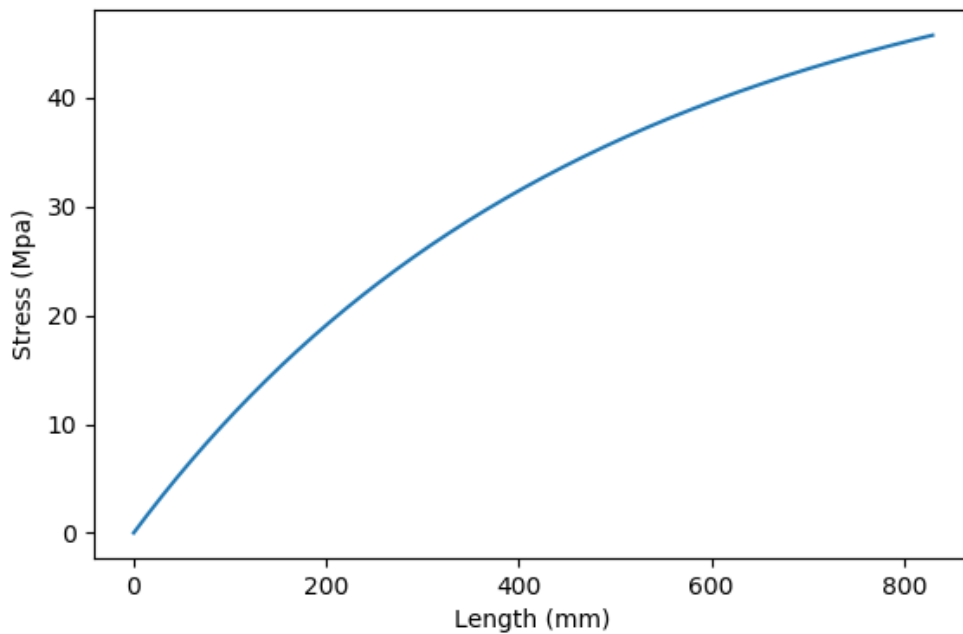
Figure 10: Bending stress along the length of the beam

3.2 Identifying distribution of strain gauges for benchmarking

To validate the results of the 3D model, a reference is needed. Using virtual strain gauges in Fedem and strain gauges on the physical rig, the accuracy of the model can be benchmarked by comparing the data. To find a good spot to put the sensors, a fatigue calculation was preformed in Fedem. The analysis was based on the standard test run defined in chapter 2. Fedem uses standard SN- curves to preform the calculation. The standard used in this case is the DNVGL RP-C203 [2]. This is a standard developed by DNVGL for designing offshore steel structures. The SN-curve B1 is chosen from this standard, which is a curve for air environment.

Figure 11 shows a section of the results from the fatigue analysis. The color coded contours represents the damage on each element of the model, where red is high and blue is low. One of the most damaged areas of the crane is on the inner boom near the connection to the tower. This is probably due to the forces sideways when the slewing motor starts and stops. Based on this analysis it was decided to put the benchmark strain gauges in this area. To avoid the uncertainties of the geometry near the welds and the possible notch effects present close to the weld, the gauges was positioned at a distance where these uncertainties were smaller.
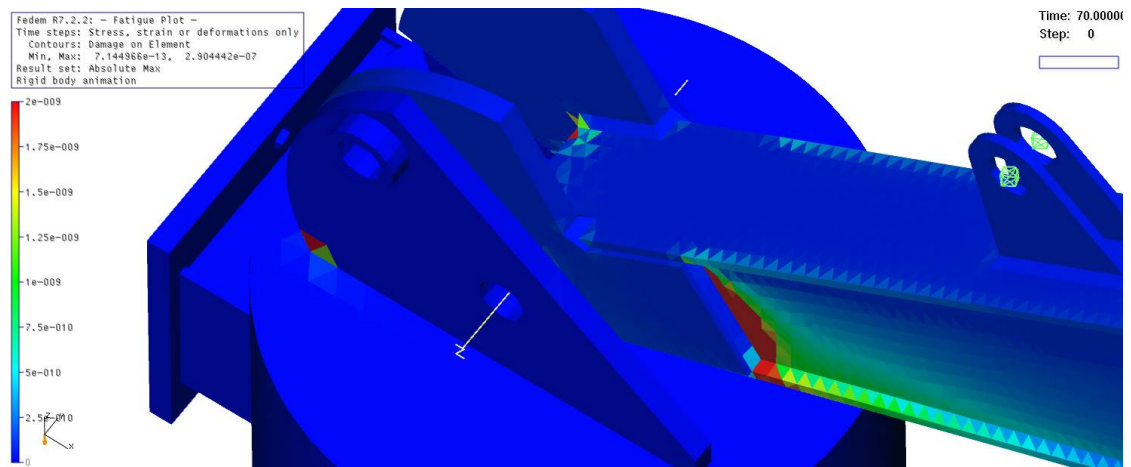
Figure 11: Results from the fatigue analysis

3.3 Equipment

The strain gauges used for the data sampling are 45 degree strain rosettes, which means that three strain gauges are oriented at 45 degrees relative to each other. A picture of the package they came in, with all the necessary data, can be seen in appendix A.2. The gauges are connected in a three wire quarter bridge configuration. A quarter bridge configuration is when one of the arms of the wheatstone bridge is active and the rest of them are fixed value resistors. The Wheatstone bridge is the sensing circuit that is used in most commercially available strain gauge instrumentation. This is due to its ability to detect small changes in resistance from the strain gauge. Three wire means that an extra wire is used to compensate for the resistance in the lead wires. A schematic of the three wire quarter bridge configuration is displayed in figure 12.

The strain gauge, labeled R_G is positioned to the left in the figure. It has two lead wires, R_{L1} and R_{L3}, connecting the strain gauge to the wheatstone bridge in a quarter bridge configuration. The wire, R_{L2}, only serves as a reference to be able to compensate for the resistance in the lead wires.
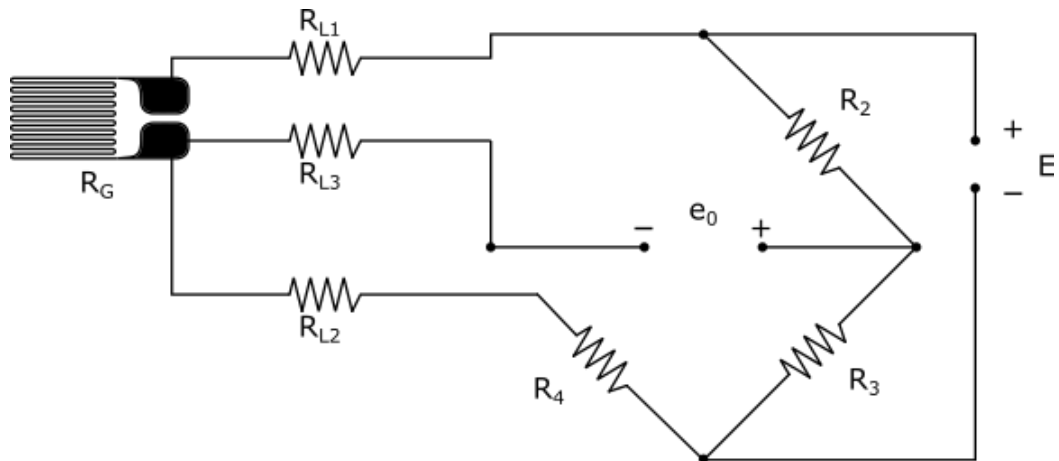
Figure 12: Schematic of a three wire quarter bridge

A 16 channel HBM QuantumX MX1615B is used to collect the data from the strain gauges. This is a universal data acquisition system that is well suited for the job. It is able to handle strain gauge connection in full, half and quarter bridge configuration at 120 and 350 ohm. A picture of the DAQ can be seen in figure 13.

Figure 13: Data acquisition amplifier

The software used to capture the data is CatmanAP, which is a data acquisition and analysis software made by HBM. It has many functions to process the data, but in this case it was only used for calibration and storing the data. The calibration of the strain gauges is done by selecting the correct configuration, in this case a three wire quarter bridge. This leads to a bridge factor of 1. The resistance of the gauges are also chosen. The ones used on the crane has 120 ohms of resistance, which is a common number. The last parameter that needs to be set is the gauge factor. The gauge factor tells how big the relative change in resistance is when the strain changes. For the gauges used on the crane this factor is 2.09. Figure 14 displays a screen shot of the user interface in CatmanAP. In the figure the settings for the channels can be inspected.

	-		Channel name		Sample rate/Filter	Slot		Sensor/Function	Zero value	Gage factor
1	◁		**MX1615_0**							
5			Oppe 0gr	▶▶	300 Hz / NA	1		SG 3 wire 120 Ohm	7077,7 µm/m	2,09
6			Oppe +45gr	▶▶	300 Hz / NA	2		SG 3 wire 120 Ohm	2013,5 µm/m	2,09
7			Oppe -45gr	▶▶	300 Hz / NA	3		SG 3 wire 120 Ohm	2571,9 µm/m	2,09
8			Nede 0gr	▶▶	300 Hz / NA	4		SG 3 wire 120 Ohm	1648,4 µm/m	2,09
9			Nede +45gr	▶▶	300 Hz / NA	5		SG 3 wire 120 Ohm	6058,6 µm/m	2,09
10			Nede -45gr	▶▶	300 Hz / NA	6		SG 3 wire 120 Ohm	-202,07 µm/m	2,09
11			Høyre 0gr	▶▶	300 Hz / NA	7		SG 3 wire 120 Ohm	1104,3 µm/m	2,09
12			Høyre +45gr	▶▶	300 Hz / NA	8		SG 3 wire 120 Ohm	7672,4 µm/m	2,09
13			Høyre -45gr	▶▶	300 Hz / NA	9		SG 3 wire 120 Ohm	1152,9 µm/m	2,09
14			Venstre 0gr	▶▶	300 Hz / NA	10		SG 3 wire 120 Ohm	1255,6 µm/m	2,09
15			Venstre +45gr	▶▶	300 Hz / NA	11		SG 3 wire 120 Ohm	2518,9 µm/m	2,09
16			Venstre -45gr	▶▶	300 Hz / NA	12		SG 3 wire 120 Ohm	2137,7 µm/m	2,09
17			B_1800	▶▶	300 Hz / NA	13		SG 3 wire 120 Ohm	118,05 µm/m	2,09
18			B_1930	▶▶	300 Hz / NA	14		SG 3 wire 120 Ohm	-475,91 µm/m	2,09
19			B_2100	▶▶	300 Hz / NA	15		SG 3 wire 120 Ohm	-1681,7 µm/m	2,09
20			B_2230	▶▶	300 Hz / NA	16	☒	Use hardware settings	508,88 µm/m	
21			MX1615_0 hardware ti			-		Hardware time channel	N.A.	
22			MX1615_0 hardware ti			-		Hardware time channel	N.A.	
23			MX1615_0 hardware ti			-		Hardware time channel	N.A.	

Figure 14: CatmanAP software

3.4 Mounting the strain gauges

The strain gauges was mounted at the positions identified previously. First the paint was grinded off at the area where each strain rosette were to be mounted. Then the areas was sanded with a fine sandpaper. The surface was cleaned with acetone, removing all dirt and fat from the area. Finally glue was applied at the exact area for the gauge, before the gauge was aligned and pressed down while the glue was curing. Later the area was covered with sticky sheets protecting the strain rosettes and the connection points for the wires from harm. The cables for each gauge was extended before they were connected to the data acquisition amplifier. The strain gauge wires were secured to the crane using strips to avoid movement. A close up of the crane with gauges mounted can be seen in figure 15.

Figure 15: Strain rosettes on the crane

3.5 Sampling data

The data acquisition amplifier was connected to a computer via ethernet cable and turned on. The system was given time to stabilize before the sampling started. This is because some change in the measurements can happen right after the system is turned on, due to a change in temperature in the strain gauges. Just before sampling the initial strain in the gauges was set to zero. All measurements was sampled with either 50 or 300 Hz sample rate. 50 Hz is enough for most cases, but to be able to capture the natural frequency of the crane 300 Hz is necessary to avoid aliasing in critical regions.

3.6 Strain rosettes

Figure 16 shows how the strain rosettes are aligned on the beam. The decision was made to mount strain rosettes on all four sides of the beam. This resulted in access of a lot more data than what was in the end used to obtain the results presented. However, it proved useful to be able to transform the strains into x-direction, y-direction and shear strain. By doing this the principal strains could be calculated by mohrs circle. This helped to find out if the alignment of the rosettes was good enough to measure the strains wanted.

Equation 8 shows the relation between the strains in the measured directions versus the x, y and shear strains. In equation 9 this is put in matrix form. The transformation matrix is called A and is calculated based on the angles in the figure and presented in equation 10. Equation 11 displays the inverse of the matrix in equation 9, which finally makes the desired calculation possible. Equation 12 shows the inverted A matrix needed to calculate ϵ_x, ϵ_y and γ_{xy}.

$$
\begin{aligned}
\epsilon_A &= \epsilon_x cos^2\theta_A + \epsilon_y sin^2\theta_A + \gamma_{xy} sin\theta_A cos\theta_A \\
\epsilon_B &= \epsilon_x cos^2\theta_B + \epsilon_y sin^2\theta_B + \gamma_{xy} sin\theta_B cos\theta_B \\
\epsilon_C &= \epsilon_x cos^2\theta_C + \epsilon_y sin^2\theta_C + \gamma_{xy} sin\theta_C cos\theta_C
\end{aligned}
\tag{8}
$$

$$
\begin{bmatrix} \epsilon_A \\ \epsilon_B \\ \epsilon_C \end{bmatrix} =
\begin{bmatrix}
cos^2\theta_A & sin^2\theta_A & sin\theta_A cos\theta_A \\
cos^2\theta_B & sin^2\theta_B & sin\theta_B cos\theta_B \\
cos^2\theta_C & sin^2\theta_C & sin\theta_C cos\theta_C
\end{bmatrix}
\begin{bmatrix} \epsilon_x \\ \epsilon_y \\ \gamma_{xy} \end{bmatrix}
\tag{9}
$$

$$
A = \begin{bmatrix}
1/2 & 1/2 & 1/2 \\
0 & 1 & 0 \\
1/2 & 1/2 & -1/2
\end{bmatrix}
\tag{10}
$$

$$
\begin{bmatrix} \epsilon_x \\ \epsilon_y \\ \gamma_{xy} \end{bmatrix} =
\begin{bmatrix} & A^{-1} & \end{bmatrix}
\begin{bmatrix} \epsilon_A \\ \epsilon_B \\ \epsilon_C \end{bmatrix}
\tag{11}
$$

$$
A^{-1} = \begin{bmatrix}
1 & -1 & 1 \\
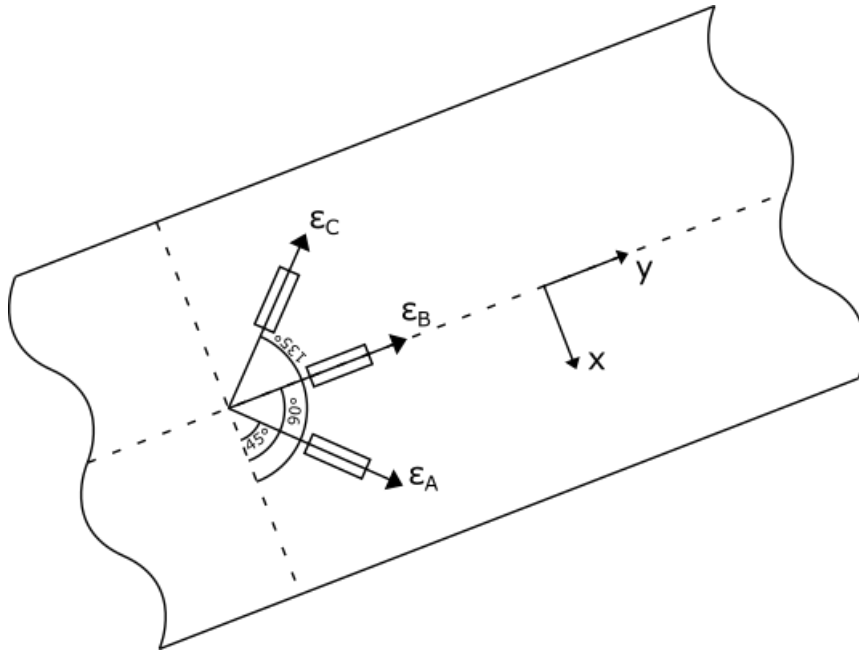0 & 1 & 0 \\
1 & 0 & -1
\end{bmatrix}
\tag{12}
$$

Figure 16: Positioning of strain rosettes

4 Natural frequency analysis

The purpose of this section is to compare eigenfrequencies from physical testing with results from simulations in Fedem. When these results are compared, an evaluation on how accurate the model is can be conducted. An eigenfrequency of a structure, also called natural frequency, is the frequency the structure tends to oscillate. The frequency relates to the stiffness matrix and mass matrix of the structure. This relation is derived from the equation for a harmonic oscillator, and is shown in equation 13.

$$\omega_n = \sqrt{k/m} \tag{13}$$

4.1 Modal analysis

A modal analysis was preformed in Fedem to find the models mode shapes and their natural frequencies. The simulation aims to find the natural frequency of the outer boom, so the rest of the crane was not needed for the simulation. Figure 17 shows the model of the boom in Fedem. The model is imported from Siemens NX where the boom was meshed. RBE2 elements are used in the holes that are being used as connection points of the boom. The part also inherits its material data assigned in the NX model. The booms connection points are modeled with revolute joints, where the axis of rotation is orientated perpendicular to the holes. These revolute joints are attached to the boom and to ground.The pulleys have been added to the model to make sure the mass matrix is correct. They are attached to the boom by revolute joints, however the rotational degree of freedom has been fixed to avoid modes in the analysis where the pulleys rotate.
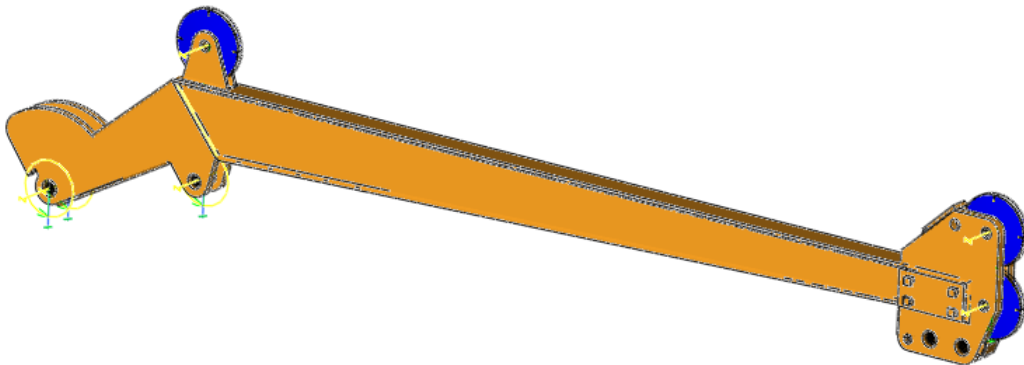

Figure 17: Model of modal analysis in fedem

The first mode has an eigenfrequency of 16.2 Hz, displayed in figure 18. The mode shape can be described as when the tip of the boom oscillates from side to side. Figure 19 shows the second mode of the simulation. The eigenfrequency of this mode is 36.3 Hz. In this mode the tip of the boom oscillates in the vertical direction, and the mode oscillating in this direction is the one of interest.
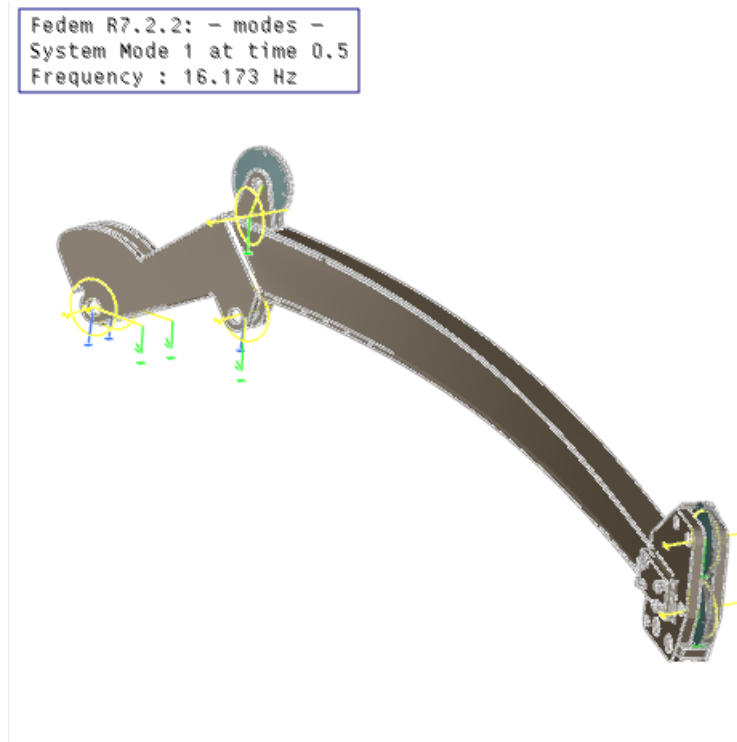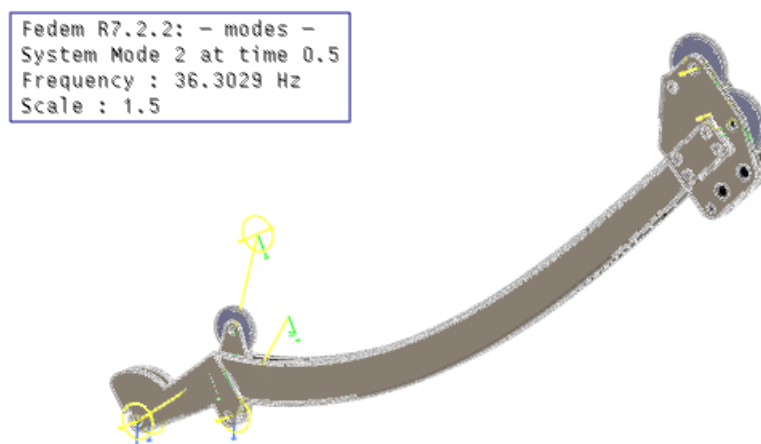

Figure 18: Mode 1 of the simulation

Figure 19: Mode 2 of the simulation

4.2   Physical testing of natural frequency

A test was conducted on the crane, where a strain gauge was used for sampling data. The strain gauge that was used is the one on top of the outer boom which is parallel to the length of the boom. The strain gauge was connected to the HBM QuantumX data acquisition amplifier system and sampled in the software Catman AP. The sample rate used during the test was 300 Hz. A square pulse was applied to the end of the boom, by the use of a nylon hammer. The stroke was made in vertical direction. Figure 20 shows the dynamic response of the test.
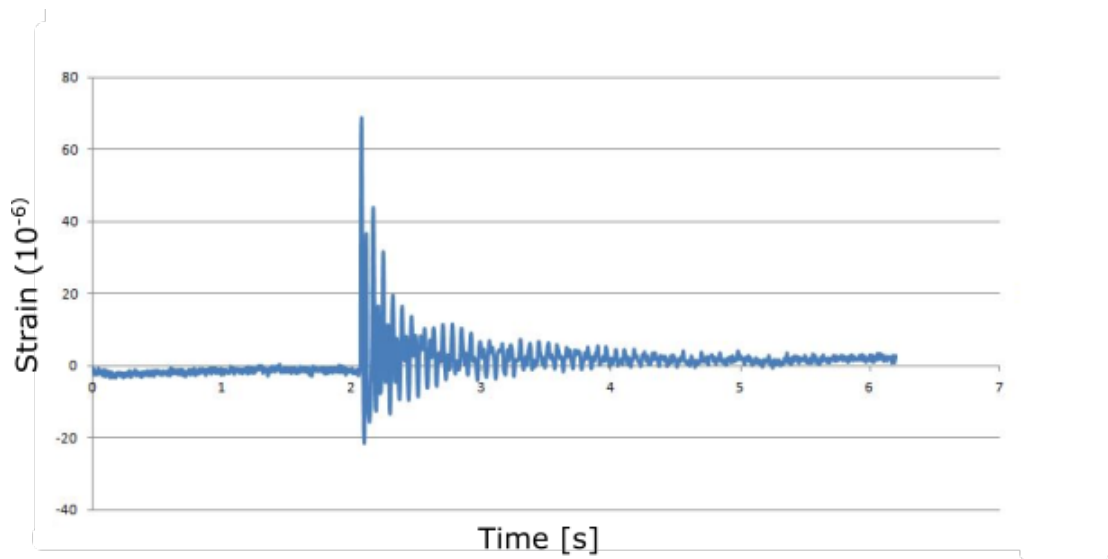
Figure 20: Oscillations of the beam

The test results was post processed to find the natural frequencies present in the oscillating boom. This was done by a fourier transform. A fourier transform transforms the data from the time domain to the frequency domain. The graph, seen in figure 21, shows along the x- axis the frequencies while the y- axis shows the magnitude of the different frequencies that appeared in the signal. The ones that dominate are the natural frequencies of the boom at different modes. The three first modes comes at frequencies 12.9 Hz, 28.1 Hz and 50.4 Hz respectively.

Figure 21: Fourier transformed frequencies

4.3 Discussion of the natural frequency results

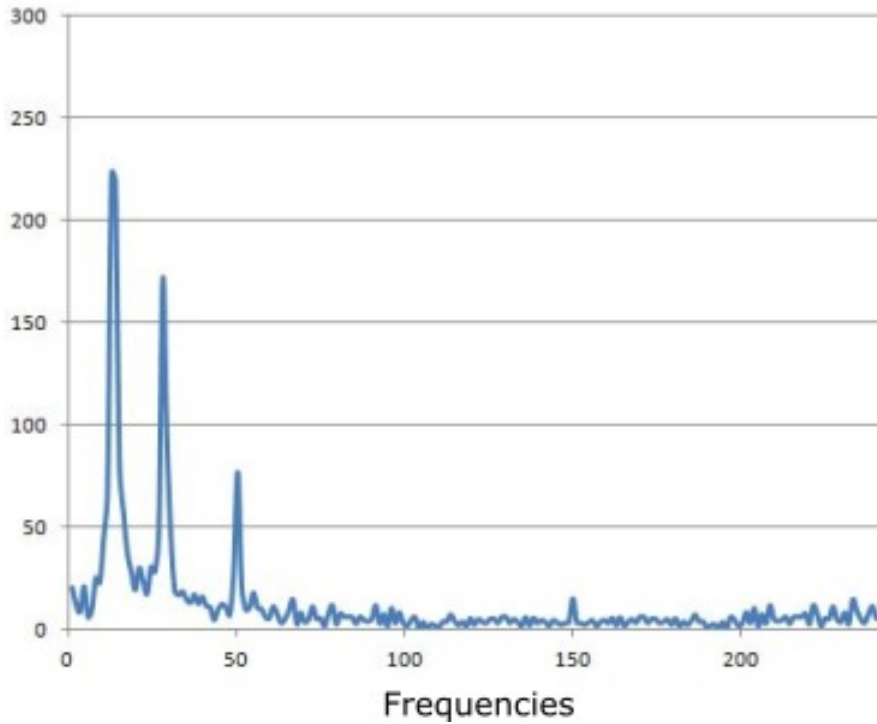The results were not as expected. The frequencies of the modal analysis are higher than the results from the fourier analysis. Other results suggest that the stiffness of the physical crane is higher than the model. If the same tendency were to be seen here, the results from physical testing should provide a higher frequency than the modal analysis. The reason for the results being as they are has to do with the boundary conditions of the model. The revolute joint to the right should have instead been modeled with a spring representing the rod on the physical crane, with a stiffness similar to the rod. The change in the boundary conditions should then contribute to produce a result with lower frequencies.

The results, as they are now, does not give any indication on how accurate the 3D modell is. However, it gives insight to how important the boundary conditions are for the accuracy of the response. This is a result worth considering when tuning the response of a model to match the physical response.

5 Development of inverse method

In this chapter the inverse method is developed. First an assessment of the geometry of the crane is preformed to know how to decompose the forces acting on the crane. Secondly a view at the cross sectional area of the crane before the final mathematical model is formulated. In the end of the chapter is a static test preformed to verify the accuracy of the mathematical model.

5.1 The geometry of the crane

Finding the angle between the beam and the horizontal plane is necessary to be able to calculate the load by the inverse method. The forces are decomposed into one force parallel to the beam and one force perpendicular to the beam and the angle is needed to find the size of the decomposed forces. This angle varies with the length of the actuator, so a function of the actuator length has to be derived. In figure 22 a wire model of the crane is displayed. The wires are drawn between the joints of the crane. The machine drawing used as a basis for the wire model can be seen in appendix A.3.
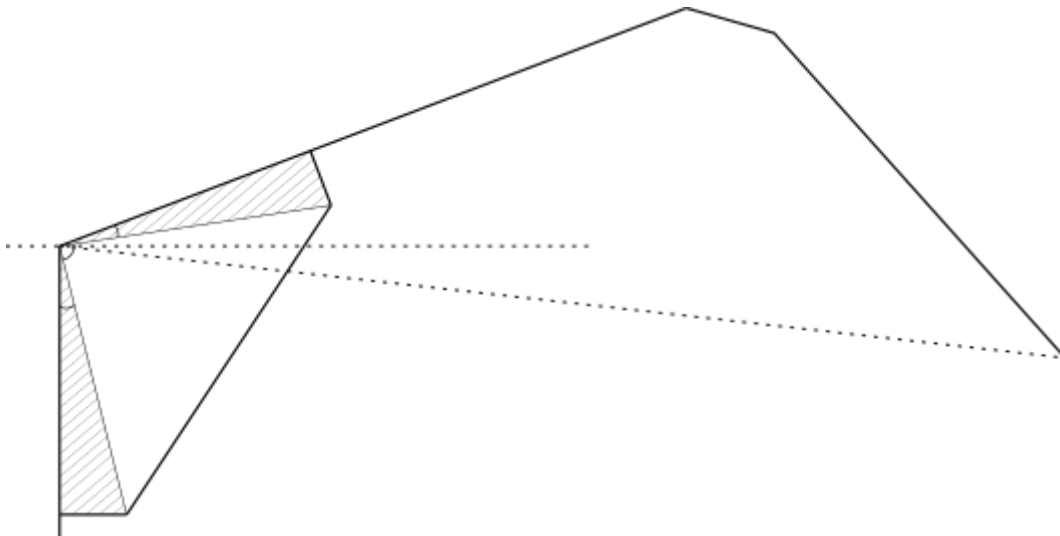

Figure 22: Wire model of the crane

In order to find the angles of the crane it is split into two parts. The first one is shown in figure 23. The line called c(t) is the actuator, which changes length with respect to time. Two right angled triangles are drawn into the figure. This makes it possible to find the distance between the three joints that makes up the triangle and thereby calculate the angle α. This angle is found by using the law of cosine, seen in equation 14. Here y is the hypotenuse of the triangle made up by the length of the tower and the distance from the center of the tower to the lower actuator joint. Likewise x is the hypotenuse of the triangle made up by the distance along the length of the boom between the two joints and the distance out to the upper joint. Equation 16 is reached by rearranging equation 14. Adding the values from equation 15, the final form is reached in equation 17.

$$c(t)^2 = x^2 + y^2 - 2xy cos\alpha \tag{14}$$

where

$$x = \sqrt{130^2 + 600.2^2} = \underline{614.12}$$
$$y = \sqrt{154.2^2 + 550^2} = \underline{571.21} \tag{15}$$

$$\alpha = cos^{-1}(\frac{x^2 + y^2 - c(t)^2}{2xy}) \tag{16}$$

resulting in

$$\alpha = cos^{-1}(\frac{703424 - c(t)^2}{701583}) \tag{17}$$
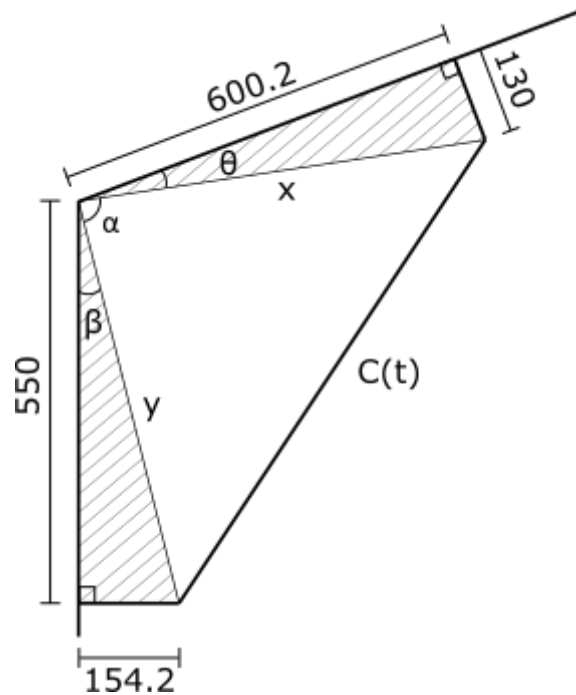
Figure 23: Model of the moving part of the crane

The second part of the calculations to find the angle is shown in figure 24. The figure displays all the measurements needed to solve the problem. The big triangle represents the two booms of the crane. The base line represents the distance between the joint, connecting the inner boom to the tower, and the end of the outer boom. Since there is no actuation changing the relative position between the booms, the whole part can be considered rigid. The small triangle in the top left of the figure is the small part of the big triangle and was needed to find the desired values.

Figure 24: Model of the rigid part of the crane

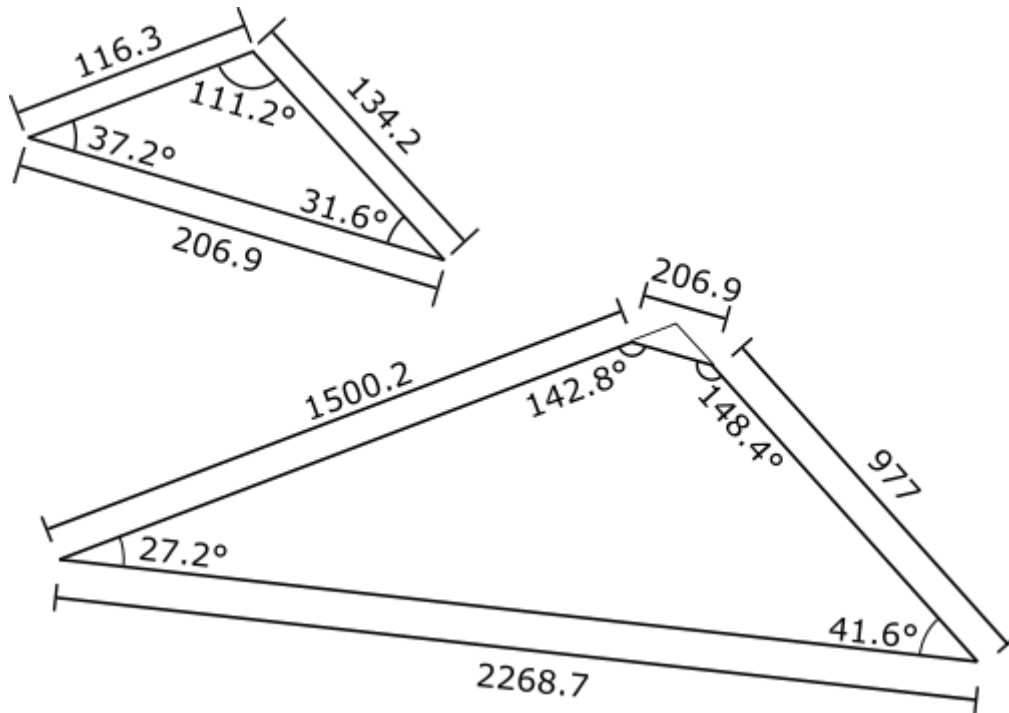Figure 25 sums up all the information needed to find the angle, φ. With this angle the forces can be decomposed. First the angle γis found, by equation 18. The approach is to find the angle between the tower and the boom and then subtract the angle of the triangle and the right angle.

$$\gamma = \beta + \alpha + \theta - 27.17° - 90° \tag{18}$$

Two horizontal dotted lines are drawn into the figure. Since these lines are parallel to each other and a third dotted line acts as a transversal, the angle γreappears on the right side of the boom because the angles are correspondent. Then the small angle to the left of the tip is also γ. This leads to equation 19.

$$\begin{aligned} \phi &= 41.63° - \gamma \\ \phi &= 41.63° - (\beta + \alpha + \theta - 27.17° - 90°) \\ \phi &= 130.92° - cos^{-1}(\frac{703424 - c(t)^2}{701583}) \end{aligned} \tag{19}$$
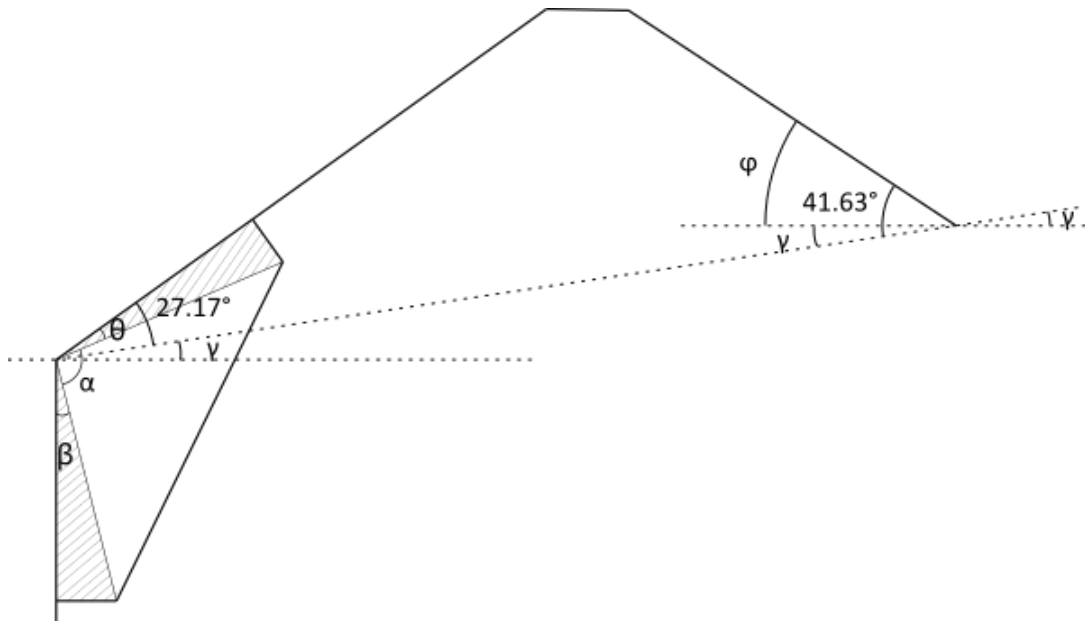

Figure 25: Wire model with resulting angles

5.2 Calculating 2nd moment of area and cross sectional area

In figure 26 is a detailed view of the cross section where the strain gauges are positioned. Remember that the cross section varies along the length of the beam. The cross section consists of several parts. The two vertical plates are called the web and have their center of area on the y axis. These plates have a significant role of moving the horizontal plates away from the y- axis. These horizontal plates are called the flanges and they contribute massively to the stiffness of the beam because of steiners theorem. In addition to these main parts, the welds also needs to be take into account. Equation 20 shows the calculation of the second moment of area with respect to the y- axis. The width of a plate is denoted with b and the height h. The subscript V is for the vertical plates, H is for the horizontal plates and W is the subscript used for the welds. Z is the distance from the y- axis to the center of area of each element. In equation 21 the cross sectional area is calculated.

$$
\begin{aligned}
I_y &= 2\frac{1}{12}b_V h_V^3 + 2(\frac{1}{12}b_H h_H^3 + z_H^2 b_H h_H) + 4(\frac{1}{36}b_W h_W^3 + z_W^2 \frac{b_W h_W}{2}) \\
&= \underline{383715mm^4}
\end{aligned}
\tag{20}
$$

$$
A = 2b_V h_V + 2b_H h_H + 4\frac{b_W h_W}{2} = \underline{600mm^2}
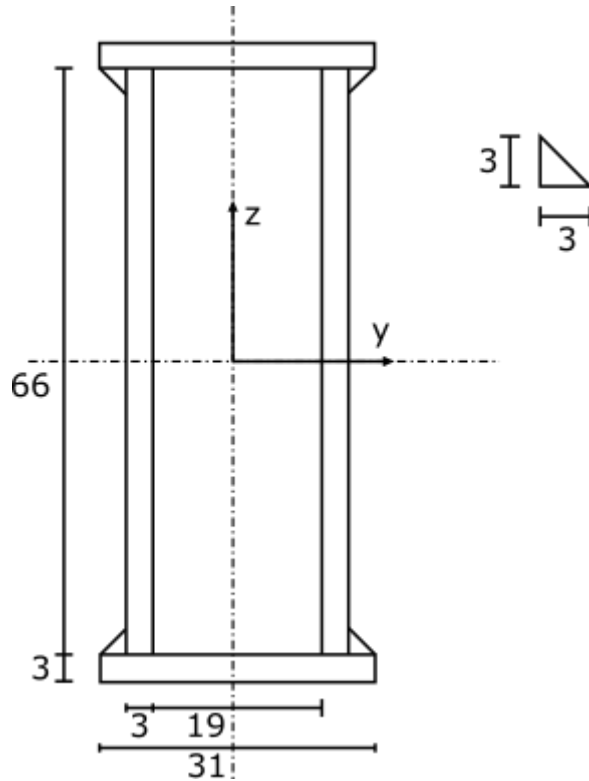\tag{21}
$$

Figure 26: Detailed cross section

5.3   Calculation of forces

The ultimate goal of these calculations is to estimate the load hanging on the crane. Only the outer boom needs to be evaluated to find the forces by the inverse method. Making these estimations precise relies on a good mathematical model. A drawing of the free body diagram, bending moment diagram and normal force diagram can be seen in figure 27. From the free body diagram it can be seen that there is a small perpendicular arm, of lenght R, from the main beam. It is there because the load is hanging from a point that does not coincide with the center line of the beam, but rather a point with distance R from the center line. The load, F, is hanging vertically from this point. This load can be decomposed into two parts. One parallel to the beam and one perpendicular to the beam. The magnitude of the decomposed forces depends on the angle between the beam and the horizontal plane, φ. This results in a normal force and perpendicular force shown in equation 22.

$$
\begin{aligned}
F_N &= F sin\phi \\
F_P &= F cos\phi
\end{aligned}
\tag{22}
$$

The main beam of the normal force diagram is only influenced by to formal force. The magnitude is constant along the length of the beam. By the use of these decomposed forces, the bending moment diagram can be drawn. The normal force induces a small bending moment in the arm, R. This increase linearly over the length R. The perpendicular force induces a bending moment on the beam starting at zero on the tip and increasing linearly over the length L of the beam. Due to equilibrium near the corner where the two lines meet, the small bending moment needs to be taken into account on the main beam. By using the super position principle, the final bending moment at the position of the strain gauges is reached and is presented in equation 23.

$$
M = FLcos\phi - FRsin\phi
\tag{23}
$$

The stresses occurring at the strain gauges is the sum of the bending stresses and the normal stresses, as described in equation 24. The stresses are a function of the elastic modulus, E, and the strain, ε. The bending stresses is a funciton of the bending moment, the 2nd moment of area calculated in a previous section, and the distance, z, from the center line out to the point of interest. The normal stresses is a function of the normal force and the area of the cross section i question. This is displayed in equation 25.

$$
\sigma = \sigma_M + \sigma_N
\tag{24}
$$

$$E\epsilon = \frac{M}{I}z + \frac{F_N}{A}$$

$$E\epsilon = \frac{FLcos\phi - FRsin\phi}{I}z + \frac{Fsin\phi}{A} \tag{25}$$

The force, F, is the only unknown. By rearranging the equation it is possible to solve the equation for F, as described by equation 26

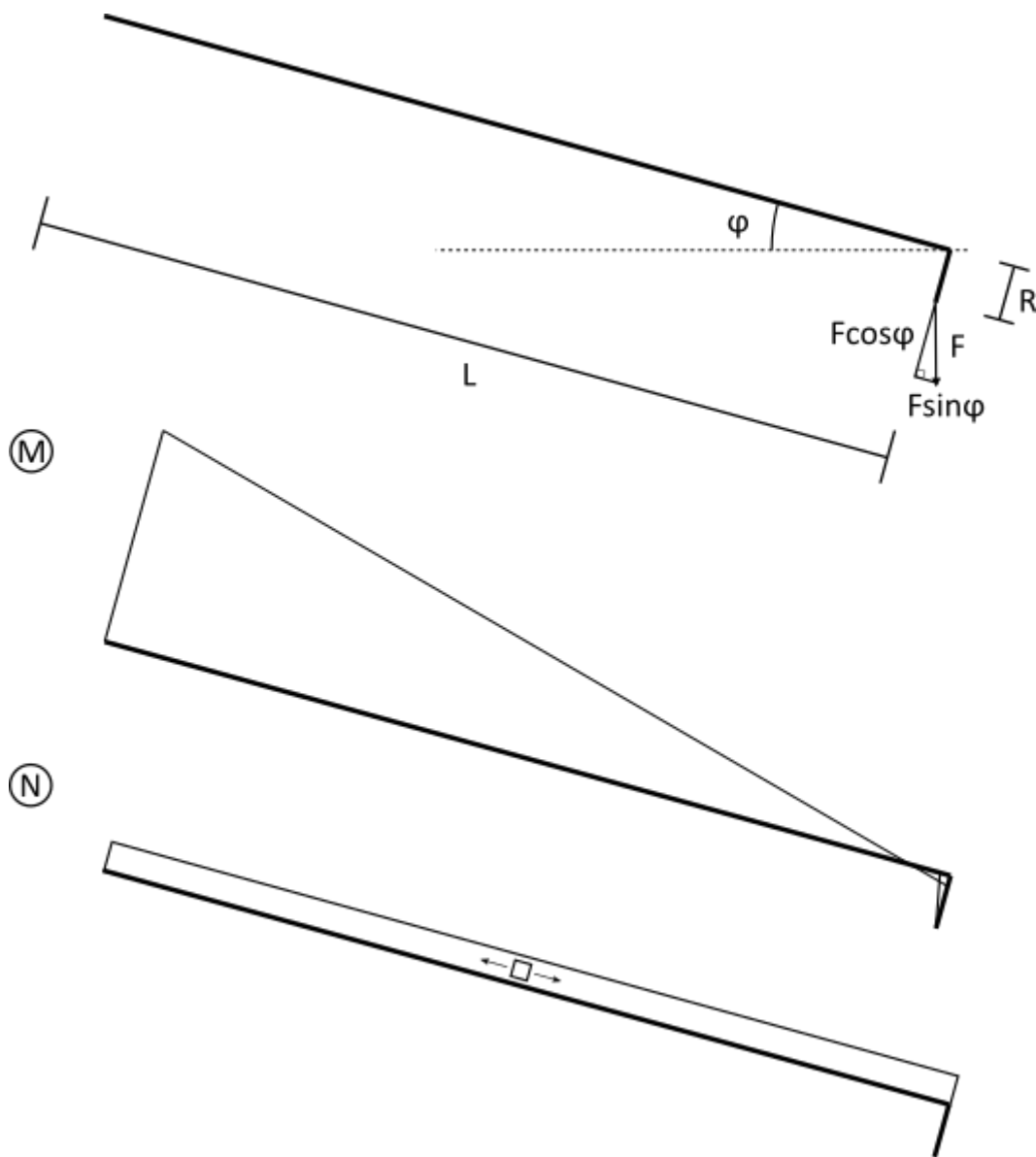$$F = \frac{E\epsilon}{\frac{Lcos\phi - Rsin\phi}{I}z + \frac{sin\phi}{A}} \tag{26}$$

Figure 27: Free body diagram, bending moment diagram and normal force diagram

5.4 Static testing

A test with static loads was conducted to assess the accuracy of the mathematical model. An example of a data set from one of these measurements can be seen in figure 28. The graph plots the data with micro strain on the y- axis, as a function of time on the x- axis. The positive curve comes from the upper strain gauge parallel to the beam, and the negative curve comes from the lower strain gauge in the same direction. While measuring it was important to make sure that the load was at rest. After the sampling, the data was averaged in a time interval where the data indicates no movement of the load. In this case an average of the data between 10 and 12 seconds was used. Testing was preformed with four different loads. The lower actuator length was 875 mm, resulting in an angle, φ, of 35.83 degrees. The other values are constants in the formula. All of the different parameters are listed in table 1.

Parameter	Value
actuator length	875mm
resulting ϕ	35.83 deg
E	210 GPa
I	383715 mm^4
z	36 mm
A	36 mm^2
g	9.81m/s^2
L	780 mm
R	56 mm

Table 1: Parameters used for calculation

For the estimation of the masses equation 26 have been divided by the gravitational acceleration on both sides, resulting in equation 27. This makes it easier to quickly compare the estimated mass to the mass applied to the crane.

$$m = \frac{E\epsilon}{(\frac{Lcos\phi - Rsin\phi}{I}z + \frac{sin\phi}{A})g} \tag{27}$$
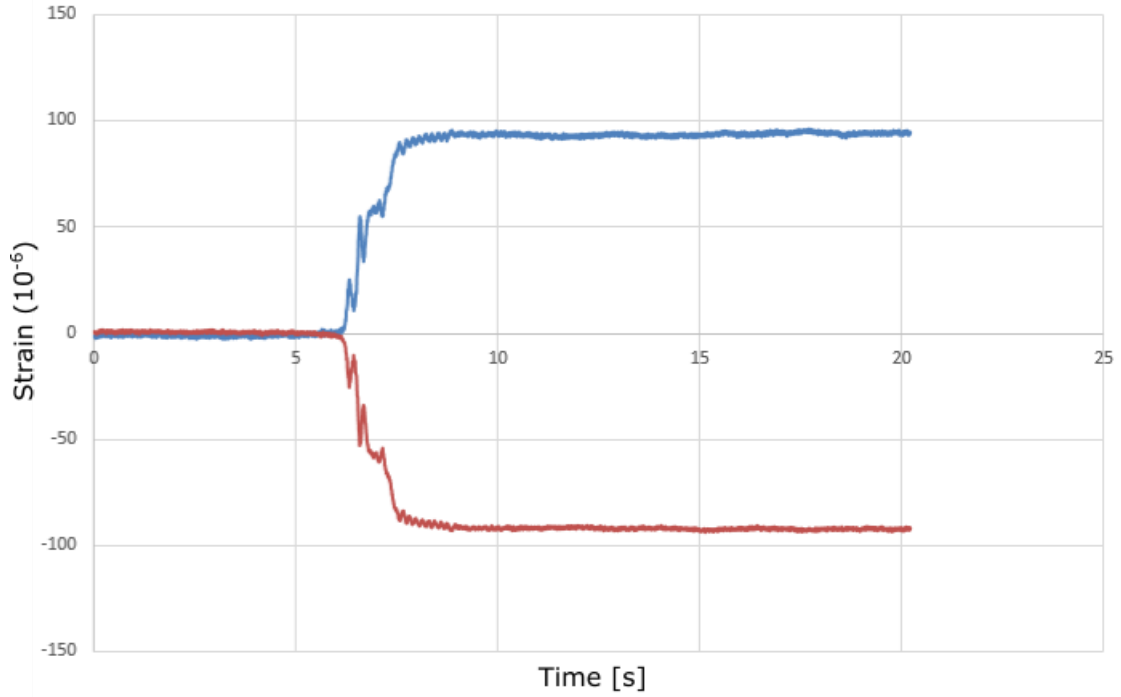
Figure 28: Data from static testing

5.5   Results from static testing

Table 2 lists the results from the static testing. The first column lists the mass
applied to each test. The strain in column two of the table comes from the upper
strain gauge and is noted in micro strains. All of the values are averages of the
upper strain gauge from a time interval of two seconds. The third column lists all
of the estimated masses based on the strains, by applying the formula in equation
27. The deviation of the estimated mass from the applied mass is listed in the last
column of the table. It reveals that all measurements results in estimated masses
that are within a 2% margin of the applied mass.

applied mass	strain (10-6)	estimated mass	deviation
21.5 kg	56.615	21.2 kg	1.4%
30 kg	81.595	30.5 kg	1.7%
35 kg	93.425	34.9 kg	0.3%
40 kg	107.39	40.2 kg	0.4%

Table 2: Mass estimation based on measured strains

5.6 Discussion of results from static testing

The static testing gave very promising results and the mathematical model will be used as it is going forward. One weakness in this particular test is that the mass was estimated only for one actuator length. However, in the next chapter the payload is estimated for the whole test run. In the static test some tuning was done to get the desired results. For example the exact cross sectional area is hard to measure precisely because the welds are a little uneven. Also the elastic modulus was tuned a little from the expected value, but the value of 210 GPa used is within what is reasonable for the material.

6 Results from simulations and testing

In this chapter the results from physical testing and simulations are presented. This inculde the strains for the inverse method, the strain for the hotspot and the results for the loads. For each presented result comes a discussion over the quality and what sources of error could be present.

6.1 Results from strains for inverse method

In figure 29 the strains related to the inverse method are plotted as a function of time. The purple and green curves are results from physical testing. The purple one comes from the upper strain gauge in the direction parallel to the beam, while the green one comes from the lower strain gauge in the same direction. Before the data was sampled the initial strains in the gauges was set to zero. The blue curve comes from the virtual strain gauge on top of the beam, in the direction parallel to the beam. The black curve comes from the lower virtual strain gauge in the same direction. In the dynamic solver in Fedem the option to preform an initial equilibrium was used. This results in an initial zero strain of the virtual strain gauges, when the crane only holds its own weight. In this way the initial conditions are the same for both physical and virtual gauges. Looking at the figure there are some deviations in the results. The deviation is roughly 12.5% when comparing the upper virtual gauge with the upper physical gauge. At around 32 seconds in the figure the upper physical strain gauge indicates a negative strain of roughly four micro strains. This also happens at the end of the run, at about 68 seconds.
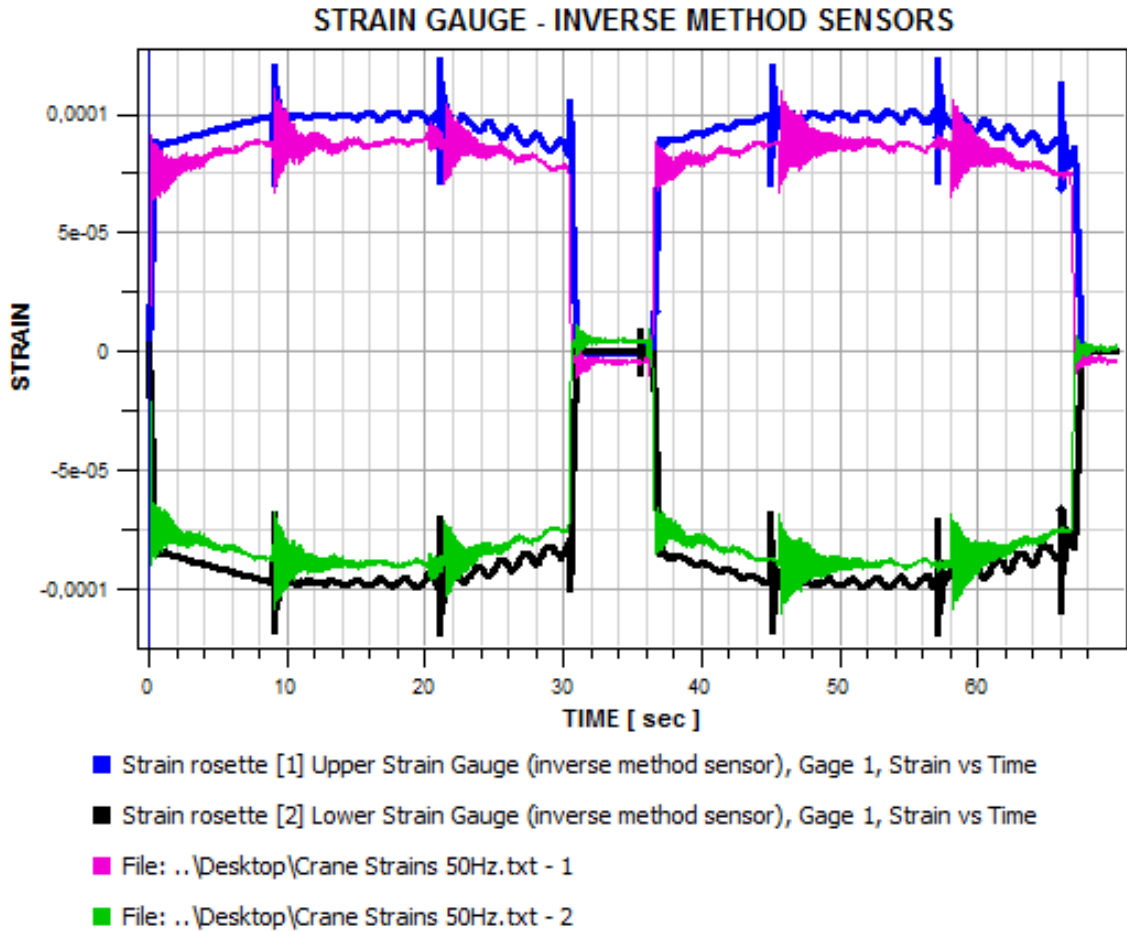
Figure 29: Results from strains for inverse method

6.2 Discussion of strains for inverse method

The curves from the physical and virtual strain gauges was expected to coincide, but as mentioned in the last section there are some deviations, roughly 12.5%. One of the sources of this deviation might be the negative strain, mentioned previously, at around 32 seconds. In this area the upper physical strain gauge indicates a negative strain of roughly four micro strains. This could be a result of drifting in the measurements made in the sample. Even tough the gauges was given time to acclimate before the testing started, there may have been some changes in the gauge making it drift a little during sampling. If four micro strains are added to all of the data points for the gauge, the data from the physical strain gauge will indicate zero strains in the area where zero strain were expected. In general, the deviations reduce to a new value of roughly 7.5%.

Another source of deviation is a difference in stiffness of the beam. In the static calculations a small increase in the elastic modulus was used, relative to the documented elastic modulus, to reach the desired results. In addition the cross sectional

area is believed to be slightly different than the model. In total the difference in stiffness is estimated to might be 3.4%. By scaling the stiffness for the two booms in Fedem by 1.034 the results in figure 30 was reached. This scaling was only used to produce the results in this figure, so no other results are scaled in this way. The results in the figure shows a deviation of 9%.

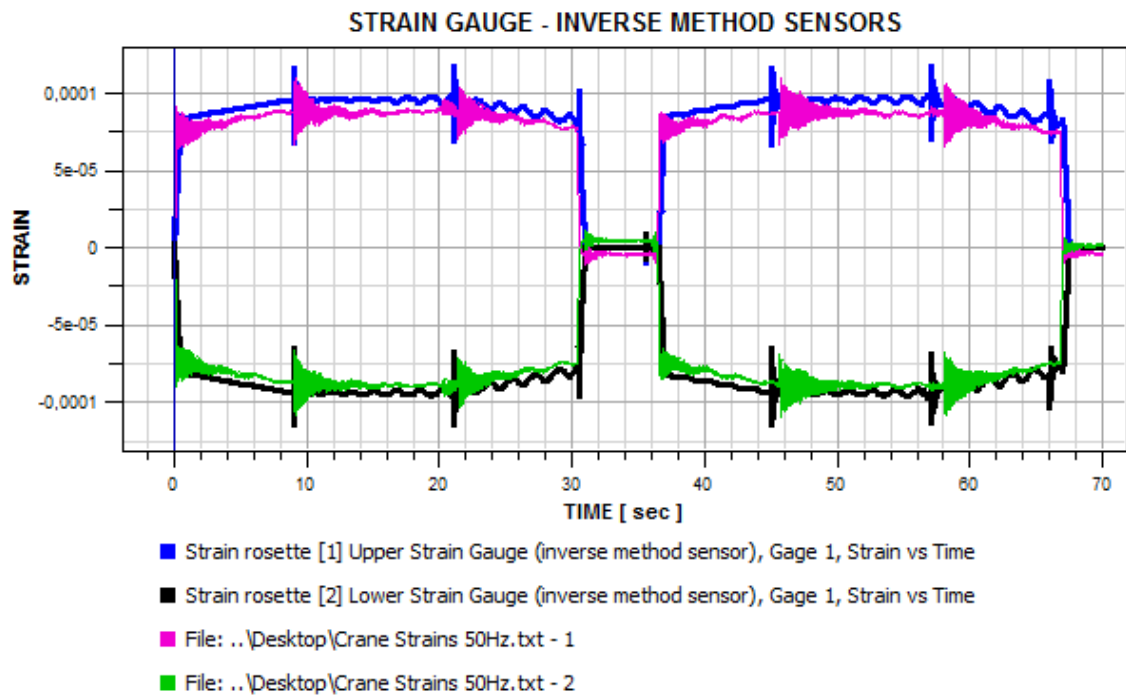By including both of the sources of deviation a new deviation of 4.3% is reached.

Figure 30: Scaled results of the strain gauges

6.3 Results from strains at hotspot

In figure 31 the strains from the hotspot are displayed. The red curve comes from
the simulation and the gauge used is the one parallel to the beam. The blue curve
is sampled from physical testing and the gauge is oriented in the same direction as
the virtual gauge in the model. There are some differences between the two curves.
In the time intervall 10- 20 seconds the strains from the virtual gauge oscillates with
a slightly larger amplitude than the strain from physical testing. The frequency is
also slightly higher. The biggest difference, however, is seen in the time intervall 20-
30 seconds. The oscillation amplitude of the virtual strain gauges are a lot bigger
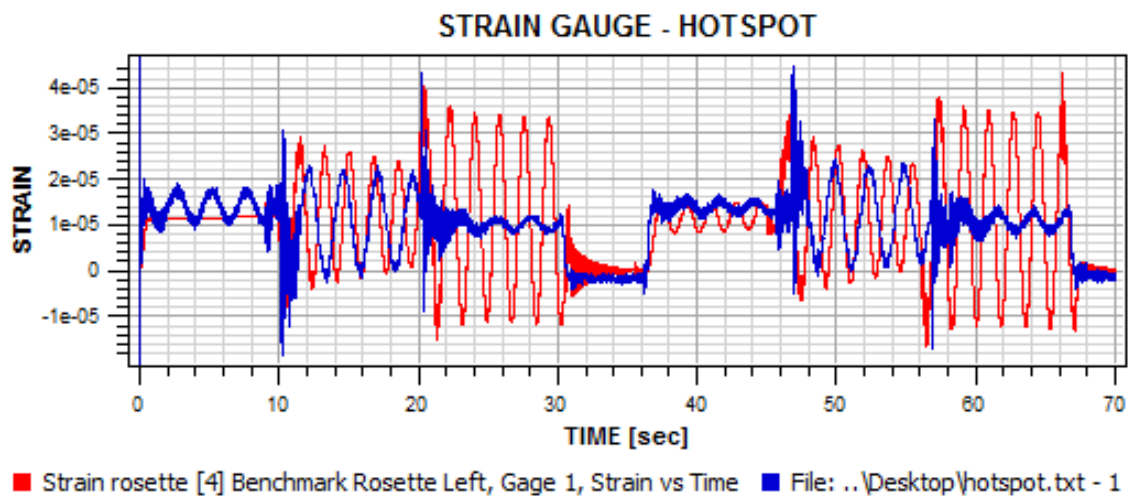than the amplitude from the physical test.

Figure 31: Results from strains at hotspot

6.4 Discussion of strains at hotspot

The biggest problem with the results in figure 31 is the deviation in the oscillations at
20- 30 seconds. As long as the deviation is this big, the model will not represent the
crane with a high enough precision. Efforts was made to reduce the amplitude of the
virtual strain gauge. As mentioned in the chapter about the model, the function for
the actuator motion was sent through a control function in order to avoid the sudden
acceleration change. This did not have much effect on these results. The believed
reason for the deviation is difference in the boundary conditions. In the model, the
joints at the connection between the inner boom and the tower are modeled to be
rigid, but on the physical crane the joints have a little looseness. At 20 seconds the
crane comes to rest after slewing. The idea is that on the physical crane most of the
energy is absorbed in the joint, while in the model the more of the energy makes
the boom oscillate. If this is the case, either the joints in the model needs to be
modeled differently or the joints on the physical crane needs to be tighter.

42

6.5 Results from calculated and simulated loads

Figure 32 displays the load acting on the crane as a function of time. The blue curve is the results from the simulation. It is plotted from the the triad at the end of the wire in the model. When the payload is lifted the curve mainly lies on a value just under 300 N, which relates to the mass of the payload times the gravitational acceleration. At some points the curve deviates from this value, which relates to dynamic effects when the actuators start and stops moving. The pink curve is calculated based on data from the physical testing. The strain gauge used for the calculation is the same used for the static calculations, the upper strain gauge parallel to the beam. The mathematical model is also the same as for the static calculations. To calculate all the points needed, the data was processed in excel. The actuator length was added for each time step based on the 3D standard test run. From the actuator length, the angle was calculated and used, along with the strain, to find the load for each time step. The curve shows that the calculated load is fairly the same over time. However the curve is positioned a little under the blue curve, and results in a slight miscalculation of the mass.
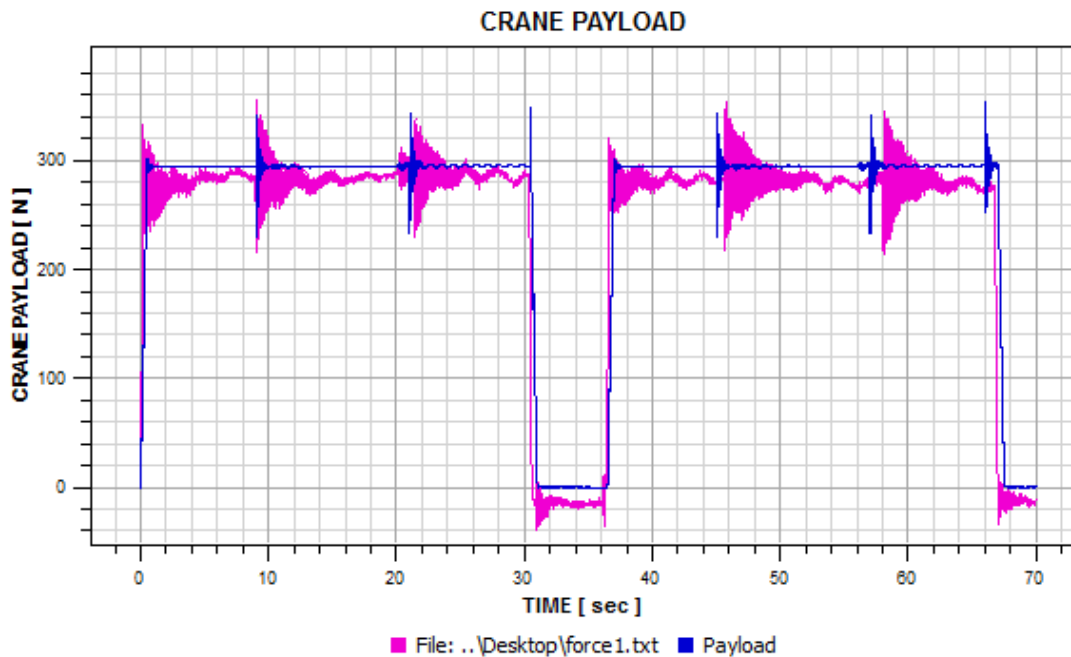

Figure 32: Comparison between simulated load and calculated load

6.6   Discussion of calculated and simulated loads

The reason for the small deviation of the calculated load from the expected value is thought to be the small error in the measurements of the strains mentioned earlier. At around 32 seconds in the graph, in figure 32, the load is calculated to be negative, which is not the case. With the basis of figure 29, the load was recalculated. The figure showed a negative strain of about four micro strains when the mass rested on the ground, at around 32 seconds in the graph. By adding the four micro strains to the strain data set for all time steps, a new adjusted data set could be used to calculate the load in the same way as before. This resulted in the curve displayed in figure 33. The blue curve is still the curve from the simulation and the green curve is the new adjusted curve based on strain data. In this graph the two curves seem to coincide. Another noticeable difference is that the green load curve is oscillating around zero when the mass is at rest on the ground, at around 32 seconds. This is what was expected rather than the negative load occurring when the data set was not adjusted. All in all the results from this calculation gives a load curve of high accuracy. However these results should be viewed with caution, as the raw data have been adjusted.
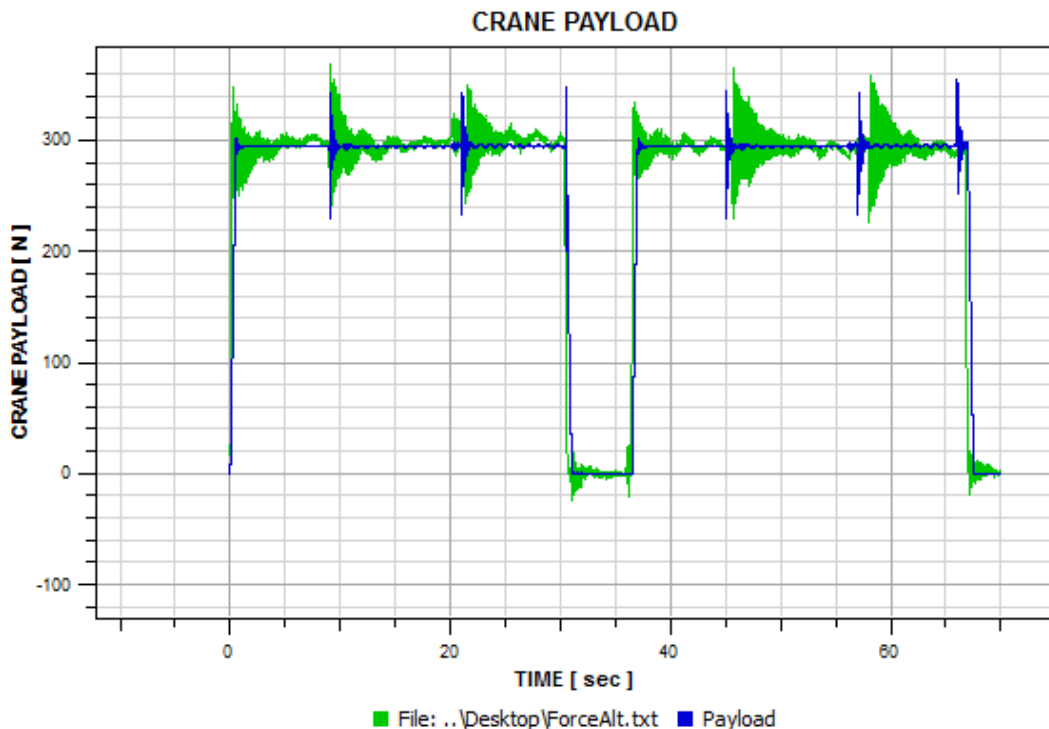

Figure 33: Comparison between adjusted load and simulated load

7 Further Work

There are still things to be done before the digital twin can be used for structural monitoring. Some suggestions are listed below.

1. Communication between to physical crane and the model needs to be set up. Data can be pulled from the actuators and sent to the model where the length change of the actuators can be defined by the data in an external function. Data from the strain gauges could be pulled by a script that calculates to load before an external function in Fedem applies it to the model.

2. Stability of strain gauge data needs to be looked into. If the goal is to send data over a long time period without interfering, drift of the data needs to be avoided. This happens when the temperature of the material in either the crane or the gauges changes. This can probably be solved by having a strain gauge as a reference that is not subjected to an external force.

3. Further work on the model needs to be done to make the response more precise. As mentioned in the previous chapter the deviations of the hotspot gauges may have something to do with the looseness of the joints in the physical crane. The joints could be modeled in a different way to make the responses more similar.

4. The inverse method has not been developed for sideways forces. This is important for when the digital model will run purely on the data received from the physical crane.

References

[1] Datta, S. *Emergence of digital twins*
https://dspace.mit.edu/handle/1721.1/104429

[2] DNVGL. *DNVGL-RP-C203 Fatigue design of offshore steel structures*
https://rules.dnvgl.com/docs/pdf/DNVGL/RP/2016-04/DNVGL-RP-C203.
pdf

A Appendix

A.1 Master thesis- task description

NTNU

Faculty of Engineering
Department of Mechanical and Industrial Engineering

Date

MASTER 2018
FOR
STUD.TECHN. ERLEND ERDAL CHRISTIANSEN

DIGITAL TWIN CRANE

Digitalt Tvilling Krane

Fedem Technology AS is developing digital twin solutions for predictive maintenance and monitoring of structural integrity. The company has therefore developed hardware and software solutions for instrumentation of physical structures and mechanisms. These solutions are currently in a prototype phase and Fedem Technology AS wants to benchmark these systems on physical twins.

Tasks include:

1. Update the FEDEM crane model (structures, wires, control system, sensors and actuators)

2. Identify an optimal distribution of sensors to capture the applied payload and responses

3. Develop inverse methods to synthesize applied loads based on physical sensor outputs

4. Instrument the physical crane based on results from task 2

5. Setup and benchmark the virtual and physical crane communication

6. Evaluate how well the sensors and inverse methods are capturing the payload on the physical crane

If time permits:

7. Benchmark the Digital twin solution with respect to identification of fatigue prediction and other failure modes

8. Write a scientific digital twin paper with the supervisors

Contact:
At the department (supervisor, co-supervisor): Terje Rølvåg and Bjørn Haugen

Address:	Org.nr. 974 767 880
	Email:
NO-7491 TRONDHEIM	mtp-info@mtp.ntnu.no
Norway	https://www.ntnu.edu/mtp

i

Norges teknisk-naturvitenskapelige universitet

From Fedem Technology AS: Runar H. Refsnæs

Vedlegg: Kontraktsmal

A.2 Strain rosettes

A.3 Machine drawing of crane